Impulse-Pilot-Aided OMP Channel Estimation for SEFDM-Based OTFS Systems

Yuanjing Qi*, Rongkun Jiang†, Nan Wu*, Dongxuan He*, Yuan Feng‡
*School of Information and Electronics, Beijing Institute of Technology, Beijing, China
†School of Integrated Circuits and Electronics, Beijing Institute of Technology, Beijing, China
‡China Research and Development Academy of Machinery Equipment, Beijing, China
Emails: jiangrongkun@bit.edu.cn

***Abstract*—Orthogonal time frequency space (OTFS) modulation offers robust performance over doubly selective channels, yet its spectral efficiency is constrained by the conventional orthogonal subcarrier spacing. To address this limitation, spectrally efficient frequency division multiplexing (SEFDM)-based OTFS intentionally compresses the subcarrier spacing in time-frequency domain to enhance spectral efficiency while retaining the delay-Doppler characteristics of OTFS, at the cost of inherent inter-carrier interference. In this paper, we propose an OMP-based sparse channel estimation framework for SEFDM-based OTFS using an impulse-pilot block at the transmitter. We obtain the corresponding dictionary by deriving the delay-Doppler (DD) domain input-output relationship of the SEFDM-based OTFS system, and address the colored-noise issue induced by subcarrier compression by adopting generalized least squares. Moreover, we derive both the Cramér-Rao lower bound (CRLB) with unknown support and the oracle CRLB with known support as theoretical performance benchmarks for the proposed channel estimation algorithm. Simulation results demonstrate that the proposed algorithm closely approaches the oracle CRLB and exhibits negligible performance variation across different packing factors.**

***Index Terms*—spectrally efficient frequency division multiplexing (SEFDM), orthogonal time frequency space (OTFS), channel estimation, orthogonal matching pursuit (OMP), Cramér-Rao lower bound (CRLB).**

I. Introduction

Orthogonal time frequency space (OTFS) modulation has attracted increasing interest for high-mobility scenarios, where strong Doppler spread and fast time-varying multipath can severely degrade traditional waveforms such as orthogonal frequency division multiplexing (OFDM) [1], [2]. By mapping information symbols to the delay-Doppler (DD) domain, OTFS represents a doubly selective channel in a more stable DD domain form, which helps enable reliable equalization and detection over a wide range of mobilities [3], [4]. However, practical OTFS systems usually follow the spectral efficiency limits of orthogonal multicarrier transmission, which can restrict bandwidth utilization when higher spectral efficiency is required [5].

To further improve bandwidth utilization, several recent studies have explored combining OTFS with non-orthogonal signaling design [6], [7]. In [6], the Faster-than-Nyquist (FTN) signaling is combined with OTFS modulation to exploit the sparse and nearly quasi-static channel representation in the DD domain, and corresponding detection methods are designed. In addition, SEFDM-based OTFS has been proposed as another non-orthogonal OTFS waveform. Compared with FTN-OTFS, SEFDM-based OTFS is more compatible with the OTFS framework, and its matrix-based processing is simpler. Although many works have studied non-orthogonal OTFS, most of which focus on detection, while channel estimation has been much less studied, especially for SEFDM-based OTFS, since accurate channel estimation is required for reliable equalization and detection.

Despite limited studies on channel estimation for SEFDM-based OTFS, many works have studied channel estimation for conventional OTFS. In [8], the authors proposed an embedded pilot-aided channel estimation method. However, the embedded pilot requires threshold setting, which may degrade the estimation accuracy. To improve performance, the sparse Bayesian learning (SBL) algorithm [9] and orthogonal matching pursuit (OMP) algorithm [10]–[12] have also been applied. Compared with OMP, SBL usually incurs much higher computational complexity while achieving similar normalized mean squared error (NMSE) performance. Moreover, these existing methods cannot be directly applied to SEFDM-based OTFS because they do not account for the inherent inter-carrier interference (ICI) introduced by the compression of subcarrier spacing [13].

In this paper, we develop an OMP-based sparse channel estimation framework for SEFDM-based OTFS, where an impulse pilot block is transmitted to facilitate channel estimation. The main contributions can be summarized as follows:

- First, we derive the DD domain input-output relationship model of the SEFDM-based OTFS system under the assumption of integer delay and Doppler shifts in a doubly selective channel, and construct the OMP dictionary based on this model.
- Second, since subcarrier compression causes colored effective noise, we replace the conventional least squares (LS) step with generalized least squares (GLS) in the OMP channel estimation.
- Third, we derive the Cram'er–Rao lower bound (CRLB) with unknown support and the oracle CRLB as theoretical benchmarks for the proposed channel estimation method.
- Finally, we assess the proposed channel estimation algorithm and the derived bounds using NMSE simulations.

The results show that the proposed method achieves NMSE close to the oracle CRLB and is robust to the compression of subcarrier spaces, with only small NMSE gaps across different packing factors.

II. SEFDM-based OTFS System

The block diagram of the considered SEFDM-based OTFS transceiver is shown in Fig. 1. It consists of an SEFDM-based OTFS modulator, a doubly selective channel, and an SEFDM-based OTFS demodulator.

A. SEFDM-based OTFS Modulation

The SEFDM-based OTFS modulation can be realized via a cascade of two-dimensional transforms. In DD domain, the quadrature phase shift keying (QPSK)-modulated symbols $x[k,l]$ with Gray mapping are allocated into an $N \times M$ DD grid, defined as:

$$\left\{ \left(\frac{k}{NT}, \frac{l}{\alpha M \Delta f} \right), k = 0, \cdots, N-1, l = 0, \cdots, M-1 \right\}, \tag{1}$$

where the QPSK constellation is defined as $\mathcal{A} = \{\pm \frac{1}{\sqrt{2}} \pm \frac{j}{\sqrt{2}}\}$. Here, NT and $\alpha M \Delta f$ determine the Doppler and delay resolutions, respectively. Accordingly, the Doppler and delay sampling intervals are $1/(NT)$ and $1/(\alpha M \Delta f)$.

The DD domain symbols $x[k,l]$ are then transformed into the time–frequency domain by using the inverse symplectic finite Fourier transform (ISFFT) as:

$$X[n,m] = \frac{1}{NM} \sum_{k=0}^{N-1} \sum_{l=0}^{M-1} x[k,l] e^{j2\pi(\frac{nk}{N} - \frac{ml}{M})}, \tag{2}$$

where $n \in \{0, \cdots, N-1\}$ and $m \in \{0, \cdots, M-1\}$.

Next, the time-frequency domain signals are converted into a continuous time waveform $s(t)$ using the modified Heisenberg transform as:

$$s(t) = \sum_{n=0}^{N-1} \sum_{m=0}^{M-1} X[n,m] g_{tx}(t-nT) e^{j2\pi m \alpha \Delta f (t-nT)}, \tag{3}$$

where $g_{tx}(t)$ is the transmit pulse shape. α is the packing factor which equals the bandwidth ratio of SEFDM modulation and OFDM modulation with the same bit rate. When α equals 1, the SEFDM-based OTFS will degenerate into conventional OFDM-based OTFS.

B. Integer Doubly Selective Channel

Typically, there are a small number of reflectors in the channel, and only the parameters of delay and Doppler are needed to model the channel in DD domain. Thus, the sparse representation of the doubly selective channel is given as:

$$h(\tau,\nu) = \sum_{i=1}^{P} h_i \delta(\tau - \tau_i) \delta(\nu - \nu_i), \tag{4}$$

where h_i denotes the complex path gain in the i-th path, $\delta(\cdot)$ denotes the Dirac delta function, and P is the number of paths. τ_i and ν_i represent the delay and Doppler shift associated with the i-th path, respectively. The taps of delay and Doppler for the i-th path can be given by

$$\tau_i = \frac{l_{\tau_i}}{M \Delta f}, \ \nu_i = \frac{k_{\nu_i}}{NT}, \tag{5}$$

where l_{τ_i} and k_{ν_i} represent the integer indexes of delay tap and Doppler tap corresponding to delay τ_i and Doppler ν_i, respectively.

C. SEFDM-based OTFS Demodulation

At the receiver, the received signal $r(t)$, expressed with the transmitted signal $s(t)$ over a doubly selective channel, is shown as:

$$r(t) = \int_\nu \int_\tau h(\tau,\nu) s(t-\tau) e^{j2\pi\nu(t-\tau)} d\tau d\nu + w(t), \tag{6}$$

where $w(t)$ denotes the additive white Gaussian noise (AWGN).

Then, the received signal $r(t)$ is transformed to a time-frequency domain signal as:

$$Y(t,f) = A_{g_{rx},r}(t,f) = \int_{t'} g_{rx}^H(t'-t) r(t') e^{-j2\pi f(t'-t)}, \tag{7}$$

where $A_{g_{rx},r}(t,f)$ is the cross-ambiguity function, $g_{rx}(t)$ denotes the receive pulse shape, and $(\cdot)^H$ is the Hermitian transpose.

After sampling $Y(t,f)$, the discrete signal $Y[n,m]$ is given as:

$$Y[n,m] = Y(t,f) \mid_{t=nT, f=\alpha m \Delta f} . \tag{8}$$

Operations (7) and (8) are referred to as the modified Wigner transform.

Finally, the SFFT is applied on the discrete signal $Y[n,m]$ to obtain the DD domain signal $y[k,l]$ as:

$$y[k,l] = \sum_{n=0}^{N-1} \sum_{m=0}^{M-1} Y[n,m] e^{-j2\pi(\frac{nk}{N} - \frac{ml}{M})}. \tag{9}$$

Although SEFDM-based OTFS improves spectral efficiency, it inherently introduces ICI at the receiver. Therefore, accurate channel estimation is essential for reliable detection and interference mitigation. Based on the modulation, channel, and demodulation steps described above, we can obtain a DD domain input-output relationship for the SEFDM-based OTFS system. This relationship is derived in Section III-A and used in the later channel estimation design.

III. Channel Estimation for SEFDM-based OTFS

In this section, we develop an impulse-pilot-aided channel estimation algorithm for SEFDM-based OTFS system to identify the integer delay and Doppler shift parameters. Owing to the sparsity of the DD domain channel, the estimation problem can be regarded as a sparse recovery problem from a linear model. As the linear model in OTFS [11], the SEFDM-based OTFS shares a similar linear model, which can be written as:

$$\mathbf{y} = \mathbf{\Psi h} + \mathbf{w}, \tag{10}$$

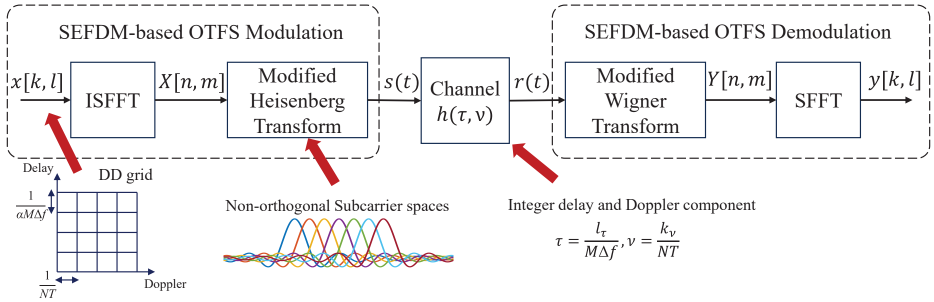

Fig. 1. The block diagram of the considered SEFDM-based OTFS transceiver.

where $\mathbf{y}$ is the received DD domain signal vector, $\mathbf{\Psi}$ is the dictionary matrix constructed by configuring possible delay-Doppler channel parameters. $\mathbf{h} = [h_1, h_2, \cdots, h_{MN}]^T$ is the channel gain in the integer delay and Doppler shift, where the channel with l_τ delay and k_ν Doppler has the gain of $h_{l_\tau * M + k_\nu}$. $\mathbf{w}$ denotes the colored effective noise after the non-orthogonal transform at the receiver.

A. Construction of Dictionary $\mathbf{\Psi}$

On the one hand, the dictionary depends on the transmitted DD domain pilot $x[k,l]$. To enhance the correlation performance, we employ an impulse pilot, i.e.,

$$x[k,l] = \begin{cases} x_p, & k = k_p, l = l_p, \\ 0, & \text{otherwise}. \end{cases} \tag{11}$$

On the other hand, the dictionary is also determined by the input-output relationship with the single channel path, which can be derived from (2)-(9) as:

$$\begin{aligned} y[k,l,k_\nu,l_\tau] = & \frac{h}{M^2} \sum_{p=0}^{M-1-l_\tau} e^{j2\pi(\frac{pk_\nu}{NM})} \mathcal{B}(p,l) \\ & \sum_{l'=0}^{M-1} \mathcal{C}(p,l') x[[k-k_\nu]_N, l'] \\ & + \frac{h}{M^2} e^{-j2\pi\frac{k-k_\nu}{N}} \sum_{p=M-l_\tau}^{M-1} e^{j2\pi(\frac{(p-M)k_\nu}{NM})} \mathcal{E}(p,l) \\ & \sum_{l'=0}^{M-1} \mathcal{C}(p,l') x[[k-k_\nu]_N, l'], \end{aligned} \tag{12}$$

where

$$\mathcal{B}(p,l) = \begin{cases} M, & (\alpha p - l + \alpha l_\tau) \in M\mathbb{Z}, \\ \frac{e^{-j2\pi(\alpha p - l + \alpha l_\tau)} - 1}{e^{-j\frac{2\pi}{M}(\alpha p - l + \alpha l_\tau)} - 1}, & \text{otherwise}, \end{cases} \tag{13}$$

$$\mathcal{C}(p,l') = \begin{cases} M, & (\alpha p - l') \in M\mathbb{Z}, \\ \frac{e^{j2\pi(\alpha p - l')} - 1}{e^{j\frac{2\pi}{M}(\alpha p - l')} - 1}, & \text{otherwise}, \end{cases} \tag{14}$$

$$\mathcal{E}(p,l) = \begin{cases} M, & (\alpha p - l + \alpha l_\tau - \alpha M) \in M\mathbb{Z}, \\ \frac{e^{j2\pi(\alpha p - l + \alpha l_\tau - \alpha M)} - 1}{e^{j\frac{2\pi}{M}(\alpha p - l + \alpha l_\tau - \alpha M)} - 1}, & \text{otherwise}. \end{cases} \tag{15}$$

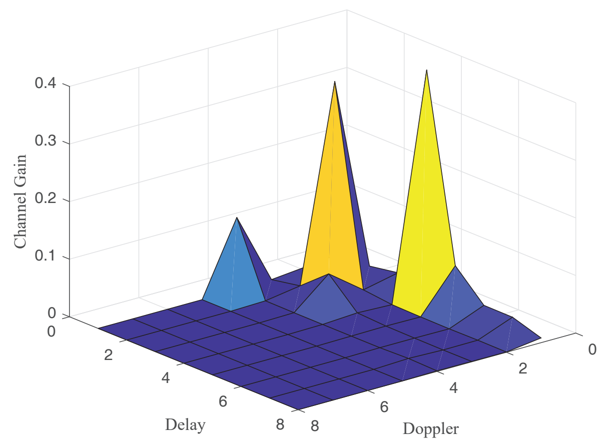

Fig. 2. Received DD domain pilot in SEFDM-based OTFS with an integer doubly selective channel.

Based on the pilot design and input-output relationship, the received DD domain pilot is illustrated in Fig. 2. It can be observed that the received signal remains impulse-like along the Doppler dimension. However, along the delay dimension, since the delay grid spacing becomes $1/(\alpha M \Delta f)$ and is no longer integer-aligned, the subcarrier compression introduces delay-domain spreading. Nevertheless, the signal energy is still concentrated around the main peak.

In summary, the dictionary $\mathbf{\Psi}$ can be constructed from (12) as:

$$\Psi(a,j) = y[k,l,k_\nu,l_\tau], \tag{16}$$

where the path gain $h = 1$, the indexes $a = l * M + k$ and $j = l_\tau * M + k_\nu$.

B. OMP Channel Estimation

The OMP algorithm iteratively identifies the column index λ^* of $\mathbf{\Psi}$ yielding the maximum correlation with the current residual, i.e.,

$$\lambda^* = \arg\max_j |\langle \mathbf{\Psi}_j, \mathbf{y}_r^t \rangle|, \tag{17}$$

Algorithm 1 Proposed impulse-pilot-aided OMP channel estimation algorithm

Input: $\mathbf{y}$, P, SEFDM-based OTFS Dictionary $\mathbf{\Psi}$, and noise covariance matrix $\mathbf{\Sigma}$.
Initialization: $\mathbf{y}_r^0 = \mathbf{y}$, $\Lambda = \emptyset$.
for $t = 0$ to $P-1$ **do**
  $\lambda^* = \arg\max_j |\langle \mathbf{\Psi}_j, \mathbf{y}_r^t \rangle|$
  $\Lambda \leftarrow \Lambda \cup \lambda^*$
  $\hat{\mathbf{h}} = (\mathbf{\Psi}_\Lambda^H \mathbf{\Sigma}^{-1} \mathbf{\Psi}_\Lambda)^{-1} \mathbf{\Psi}_\Lambda^H \mathbf{\Sigma}^{-1} \mathbf{y}$
  $\mathbf{y}_r^{t+1} = \mathbf{y} - \mathbf{\Psi}_\Lambda \hat{\mathbf{h}}_\Lambda$
end for
Output: support set Λ, and channel gains $\hat{\mathbf{h}}_\Lambda$.

where $\langle \cdot, \cdot \rangle$ denotes the inner product, i.e., $\langle \mathbf{c}, \mathbf{d} \rangle = \mathbf{c}^H \mathbf{d}$, and $\mathbf{y}_r^t$ is the residual signal at the t-th iteration. Then, the selected index is added in a support set $\Lambda \leftarrow \Lambda \cup \lambda^*$.

To handle the colored noise in the received DD domain, a GLS refinement [14] is performed as:

$$\hat{\mathbf{h}}_\Lambda = (\mathbf{\Psi}_\Lambda^H \mathbf{\Sigma}^{-1} \mathbf{\Psi}_\Lambda)^{-1} \mathbf{\Psi}_\Lambda^H \mathbf{\Sigma}^{-1} \mathbf{y}, \tag{18}$$

where $\mathbf{\Sigma}$ is the noise covariance matrix of $\mathbf{w}$ in (10), and $\mathbf{\Psi}_\Lambda$ is the submatrix of dictionary indexed by Λ. The residual is then updated by

$$\mathbf{y}_r^{t+1} = \mathbf{y} - \mathbf{\Psi}_\Lambda \hat{\mathbf{h}}_\Lambda. \tag{19}$$

When the number of channel paths is known, the OMP iteration number is set to P. When the sparsity level is unknown, a residual-based stopping rule is used. In practice, the threshold can be chosen according to the noise level and the observation dimension. The proposed impulse-pilot-aided OMP algorithm with known channel paths is shown in **Algorithm** 1.

C. Complexity Analysis

For the proposed algorithm, the correlation step in (17) has the computational complexity $\mathcal{O}(M^2N^2)$. Since $\mathbf{\Sigma}^{-1}$ is known a priori and can be precomputed, the GLS refinement in (18) and the residual update in (19) have the computational complexity of $\mathcal{O}(M^2N^2 + M^2N^2b + MNb^2 + b^3 + 2MNb)$ in the b-th iteration. Therefore, the total computational complexity over P iterations is $\mathcal{O}(2PM^2N^2 + M^2N^2b_1 + MNb_2 + b_3 + 2MNb_1)$, where $b_i = \sum_{b=1}^{P} b^i$.

IV. Cramér-Rao Lower Bound Analysis

In this section, we derive the CRLB for impulse-pilot-aided channel estimation in SEFDM-based OTFS. The CRLB provides a performance benchmark based on the Fisher information matrix (FIM) and is evaluated under an integer delay-Doppler channel model as defined in (5).

A. CRLB with Unknown Support

To obtain the CRLB for the unknown channel parameters, we compute the FIM, defined as:

$$\mathbf{J}(\boldsymbol{\theta}) = \mathbb{E}\left\{ \left[\frac{\partial}{\partial \boldsymbol{\theta}} \ln p(\mathbf{y}|\boldsymbol{\theta}) \right] \left[\frac{\partial}{\partial \boldsymbol{\theta}} \ln p(\mathbf{y}|\boldsymbol{\theta}) \right]^T \right\}, \tag{20}$$

where $p(\mathbf{y}|\boldsymbol{\theta})$ is the likelihood function of $\mathbf{y}$ given the real-valued parameter vector

$$\boldsymbol{\theta} = \begin{bmatrix} \Re\{\mathbf{h}\} \\ \Im\{\mathbf{h}\} \end{bmatrix}. \tag{21}$$

Assume the linear observation model in (10) with $\mathbf{w} \sim \mathcal{CN}(\mathbf{0}, \mathbf{\Sigma})$. Then $\mathbf{y} \sim \mathcal{CN}(\mathbf{\Psi}\mathbf{h}, \mathbf{\Sigma})$ and the likelihood is

$$p(\mathbf{y}|\mathbf{h}) = \frac{1}{\pi^{NM} \det(\mathbf{\Sigma})} \exp\big(-(\mathbf{y} - \mathbf{\Psi}\mathbf{h})^H \mathbf{\Sigma}^{-1} (\mathbf{y} - \mathbf{\Psi}\mathbf{h}) \big). \tag{22}$$

Accordingly, the log-likelihood function with respect to $\boldsymbol{\theta}$ can be written as:

$$f(\boldsymbol{\theta}) = \ln p(\mathbf{y}|\boldsymbol{\theta}) = -(\mathbf{y} - \boldsymbol{\mu}(\boldsymbol{\theta}))^H \mathbf{\Sigma}^{-1} (\mathbf{y} - \boldsymbol{\mu}(\boldsymbol{\theta})) - C, \tag{23}$$

where C is a constant term independent of $\boldsymbol{\theta}$, and $\boldsymbol{\mu}(\boldsymbol{\theta}) = \mathbf{\Psi}\mathbf{h}(\boldsymbol{\theta})$ denotes the mean of $\mathbf{y}$.

Based on (23), the first-order derivative with respect to the i-th element θ_i is

$$\frac{\partial f}{\partial \theta_i} = -(\mathbf{y} - \boldsymbol{\mu})^H \mathbf{\Sigma}^{-1} \frac{\partial \boldsymbol{\mu}}{\partial \theta_i} - \left(\frac{\partial \boldsymbol{\mu}}{\partial \theta_i} \right)^H \mathbf{\Sigma}^{-1} (\mathbf{y} - \boldsymbol{\mu}), \tag{24}$$

where $\boldsymbol{\mu} = \boldsymbol{\mu}(\boldsymbol{\theta})$. Since $\mathbb{E}\{\mathbf{y} - \boldsymbol{\mu}\} = \mathbf{0}$, we have $\mathbb{E}\{\partial f / \partial \theta_i\} = 0$. Furthermore, using the standard identity for proper complex Gaussian models with a mean that depends on the parameters and a covariance matrix independent of the parameters, the (i, j)-th element of the FIM can be expressed as:

$$J_{i,j} = -\mathbb{E}\left\{ \frac{\partial^2 f}{\partial \theta_i \, \partial \theta_j} \right\} = 2\, \Re\left\{ \left(\frac{\partial \boldsymbol{\mu}}{\partial \theta_i} \right)^H \mathbf{\Sigma}^{-1} \left(\frac{\partial \boldsymbol{\mu}}{\partial \theta_j} \right) \right\}. \tag{25}$$

Now let $\mathbf{h} = \mathbf{h}_\mathrm{R} + j\mathbf{h}_\mathrm{I}$, where $\mathbf{h}_\mathrm{R} = \Re\{\mathbf{h}\}$ and $\mathbf{h}_\mathrm{I} = \Im\{\mathbf{h}\}$. Then $\boldsymbol{\mu} = \mathbf{\Psi}(\mathbf{h}_\mathrm{R} + j\mathbf{h}_\mathrm{I})$, which yields

$$\frac{\partial \boldsymbol{\mu}}{\partial \mathbf{h}_\mathrm{R}} = \mathbf{\Psi}, \qquad \frac{\partial \boldsymbol{\mu}}{\partial \mathbf{h}_\mathrm{I}} = j\mathbf{\Psi}. \tag{26}$$

Substituting (26) into (25) gives the FIM as:

$$\mathbf{J}(\boldsymbol{\theta}) = 2 \begin{bmatrix} \Re\{\mathbf{\Psi}^H \mathbf{\Sigma}^{-1} \mathbf{\Psi}\} & -\Im\{\mathbf{\Psi}^H \mathbf{\Sigma}^{-1} \mathbf{\Psi}\} \\ \Im\{\mathbf{\Psi}^H \mathbf{\Sigma}^{-1} \mathbf{\Psi}\} & \Re\{\mathbf{\Psi}^H \mathbf{\Sigma}^{-1} \mathbf{\Psi}\} \end{bmatrix}. \tag{27}$$

Finally, the error covariance of estimator $\widehat{\boldsymbol{\theta}}$ satisfies

$$\mathbb{E}\Big[(\widehat{\boldsymbol{\theta}} - \boldsymbol{\theta})(\widehat{\boldsymbol{\theta}} - \boldsymbol{\theta})^T \Big] \succeq \mathbf{J}(\boldsymbol{\theta})^{-1}. \tag{28}$$

B. Oracle CRLB with Known Support

In sparse DD domain doubly selective channels, $\mathbf{h}$ typically has P nonzero entries with an unknown support set $\mathcal{S} \subset \{1, \ldots, MN\}$, $|\mathcal{S}| = P$. Since $\mathbf{h}$ is sparse, adopting the oracle CRLB under the sparsity assumption yields a tighter performance bound than the CRLB with unknown support [15]. If the true support $\mathcal{S}$ is known a priori, the observation model reduces to

$$\mathbf{y} = \mathbf{\Psi}_\mathcal{S} \mathbf{h}_\mathcal{S} + \mathbf{w}, \tag{29}$$

where $\mathbf{\Psi}_\mathcal{S} \in \mathbb{C}^{MN \times P}$ is the submatrix formed by the columns of $\mathbf{\Psi}$ indexed by $\mathcal{S}$, and $\mathbf{h}_\mathcal{S} \in \mathbb{C}^{P \times 1}$ collects the nonzero coefficients. Defining the real-valued parameter vector

$$\boldsymbol{\theta}_\mathcal{S} = \begin{bmatrix} \Re\{\mathbf{h}_\mathcal{S}\} \\ \Im\{\mathbf{h}_\mathcal{S}\} \end{bmatrix}, \tag{30}$$

the FIM follows the same form as (27) with $\mathbf{\Psi}$ replaced by $\mathbf{\Psi}_{\mathcal{S}}$

$$\mathbf{J}(\boldsymbol{\theta}_{\mathcal{S}}) = 2\begin{bmatrix} \Re\{\mathbf{\Psi}_{\mathcal{S}}^{H}\mathbf{\Sigma}^{-1}\mathbf{\Psi}_{\mathcal{S}}\} & -\Im\{\mathbf{\Psi}_{\mathcal{S}}^{H}\mathbf{\Sigma}^{-1}\mathbf{\Psi}_{\mathcal{S}}\} \\ \Im\{\mathbf{\Psi}_{\mathcal{S}}^{H}\mathbf{\Sigma}^{-1}\mathbf{\Psi}_{\mathcal{S}}\} & \Re\{\mathbf{\Psi}_{\mathcal{S}}^{H}\mathbf{\Sigma}^{-1}\mathbf{\Psi}_{\mathcal{S}}\} \end{bmatrix}. \quad (31)$$

Therefore, for the estimator $\widehat{\boldsymbol{\theta}}_{\mathcal{S}}$ of $\boldsymbol{\theta}_{\mathcal{S}}$,

$$\mathbb{E}\Big[(\widehat{\boldsymbol{\theta}}_{\mathcal{S}} - \boldsymbol{\theta}_{\mathcal{S}})(\widehat{\boldsymbol{\theta}}_{\mathcal{S}} - \boldsymbol{\theta}_{\mathcal{S}})^{T}\Big] \succeq \mathbf{J}(\boldsymbol{\theta}_{\mathcal{S}})^{-1}. \quad (32)$$

This oracle bound uses the support information and therefore serves as a useful benchmark for the sparse channel estimation algorithms. Such algorithms typically first estimate the support and then estimate the corresponding nonzero coefficients, as in **Algorithm** 1.

V. Simulation Results

In this section, we validate the proposed OMP channel estimation algorithm and the derived CRLB for the SEFDM-based OTFS system. The performance is evaluated in terms of the NMSE of the estimated channel vector, defined by

$$\text{NMSE} = \frac{\mathbb{E}\Big[\|\hat{\mathbf{h}} - \mathbf{h}\|_2^2\Big]}{\mathbb{E}\Big[\|\mathbf{h}\|_2^2\Big]}, \quad (33)$$

and the corresponding NMSE of the bounds, namely the CRLB with unknown support NMSE_U and the oracle CRLB NMSE_O, are used as benchmarks and defined as:

$$\text{NMSE}_U = \frac{\text{tr}\Big(\mathbf{J}(\boldsymbol{\theta})^{-1}\Big)}{\mathbb{E}\Big[\|\mathbf{h}\|_2^2\Big]}, \quad (34)$$

and

$$\text{NMSE}_O = \frac{\text{tr}\Big(\mathbf{J}(\boldsymbol{\theta}_{\mathcal{S}})^{-1}\Big)}{\mathbb{E}\Big[\|\mathbf{h}\|_2^2\Big]}, \quad (35)$$

respectively. The system parameters are set as follows. The channel is modeled as an integer doubly selective channel. Specifically, the maximum number of channel paths is set to $P = 4$, with the maximum delay index $l_{\tau,\max} = 3$ and the maximum Doppler index $k_{\nu,\max} = 3$. The delay and Doppler indices of each path are randomly generated according to a uniform distribution within the specified ranges. For each realization, the complex path gains are drawn as independent random complex coefficients, and the overall channel power is normalized.

For the proposed OMP channel estimator, Fig. 3 illustrates the NMSE performance under the setting of $N = 8$ and $M = 8$. The results are under different packing factor α and for two stopping cases: *known P* means that the OMP iterations are fixed to the true sparsity level, whereas *unknown P* indicates that the algorithm stops according to a residual-based criterion. The NMSE decreases monotonically with the increase of E_b/N_0. For different packing factor α, a slight NMSE increase is observed as α decreases, indicating that subcarrier compression only marginally affects the proposed OMP algorithm and thus demonstrating its robustness against

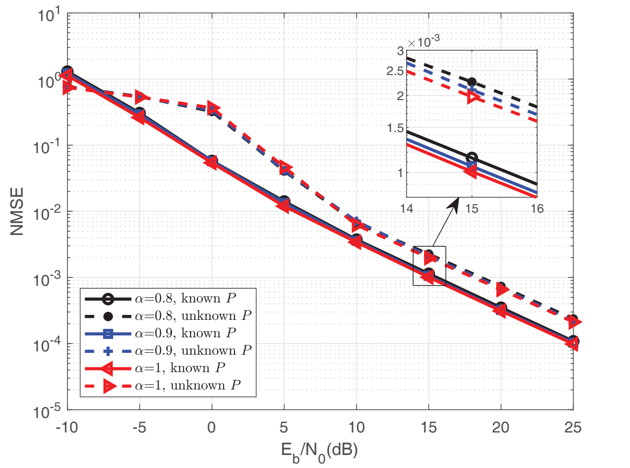

Fig. 3. NMSE performance of the proposed OMP-based channel estimation for SEFDM-based OTFS under different α.

non-orthogonality. In addition, at low E_b/N_0, *known P* is slightly worse than *unknown P* because fixing the iteration number forces OMP to select P even when the residual is dominated by noise, which increases the probability of picking wrong atoms and leads to noise overfitting; in contrast, the residual-based stopping rule may terminate earlier and avoid unnecessary iterations.

We investigate the impact of the symbol size on the proposed OMP algorithm for $N \in \{12, 20, 28\}$. The packing factor is $\alpha = 0.8$. The results show that the increasing N consistently improves the estimation accuracy, since the larger symbol size provides more observations and improves the effective sensing diversity for sparse recovery. For each N, the proposed OMP closely tracks the corresponding oracle CRLB. Moreover, in low E_b/N_0, the OMP algorithm with bigger N is closer to the corresponding oracle, which indicates that a larger amount of data leads to stronger correlation reliability, thereby increasing the probability that OMP selects the correct dictionary atoms in SEFDM-based OTFS system.

In Fig. 5, we compare the NMSE performance of different channel estimation algorithms for the SEFDM-based OTFS system. The packing factor is set as $\alpha = 0.8$, and $N = 8$, $M = 8$. The LS estimator represents a non-sparsity-aware approach without exploiting any support information, which is much worse than the sparse estimation algorithms. The proposed OMP using the derived SEFDM-based OTFS dictionary significantly outperforms LS and achieves an NMSE very close to Oracle LS. When the true support is assumed known, Oracle LS also with a derived SEFDM-based OTFS dictionary provides a substantial gain and closely approaches the oracle CRLB, serving as an upper performance reference for sparse-recovery based methods. Moreover, OMP with a mismatched dictionary suffers from a pronounced error floor, indicating that the dictionary must consider the inherent ICI in SEFDM-based OTFS modulation to achieve performance close to the oracle CRLB. Finally, the oracle CRLB is tighter

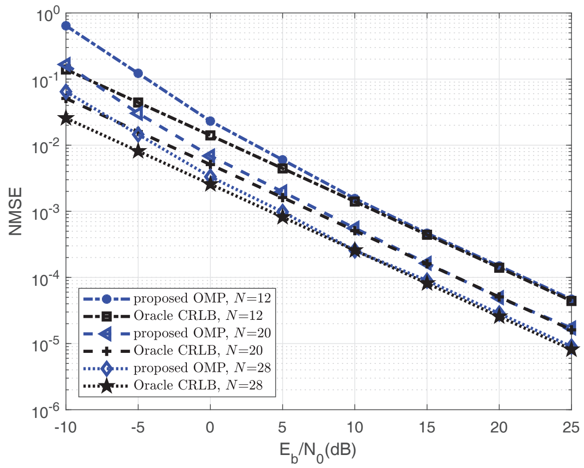

Fig. 4. NMSE comparison between proposed OMP and oracle CRLB under different symbol size N.

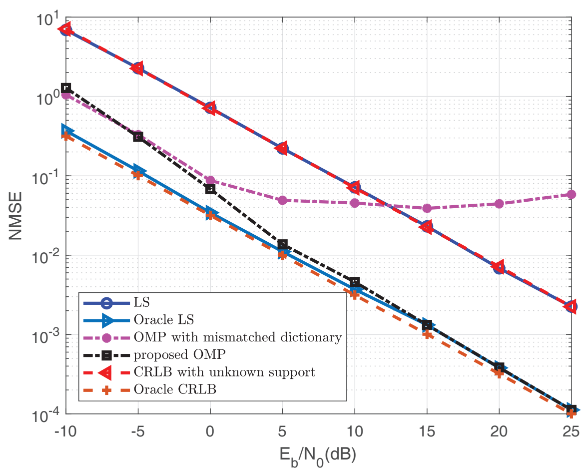

Fig. 5. NMSE comparison under different channel estimation algorithms and CRLBs.

for the sparse channel estimation, highlighting the performance gain that can be achieved when sparsity support information is exploited.

VI. Conclusion

This paper investigated impulse-pilot-aided channel estimation for SEFDM-based OTFS over integer doubly selective channels. By explicitly incorporating the SEFDM-induced non-orthogonal coupling into the end-to-end input-output relation, we derived a matched sensing dictionary and developed an OMP-based sparse channel estimation algorithm. We further established CRLB benchmarks under both unknown support CRLB and oracle CRLB assumptions to characterize the performance limits. Simulation results demonstrated that the proposed OMP algorithm for SEFDM-based OTFS significantly outperforms LS and mismatched-dictionary OMP, and approaches the oracle CRLB. In addition, the algorithm has been shown to be robust to subcarrier compression. These results validate the effectiveness of the proposed approach and provide useful guidelines for the channel estimation in SEFDM-based OTFS system. In future work, we will investigate channel estimation in the presence of fractional Doppler spread and explore more advanced support recovery methods to further enhance the estimation performance.

References

[1] R. Hadani et al., "Orthogonal time frequency space modulation," in *Proc. IEEE Wireless Commun. Netw. Conf. (WCNC)*, Mar. 2017, pp. 1–6.

[2] P. Raviteja, K. T. Phan, Y. Hong, and E. Viterbo, "Interference cancellation and iterative detection for orthogonal time frequency space modulation," *IEEE Trans. Wireless Commun.*, vol. 17, no. 10, pp. 6501–6515, Oct. 2018.

[3] N. Wu, H. Li, D. He, A. Nallanathan, and T. Q. S. Quek, "Integrated sensing and communication receiver design for OTFS-based MIMO system: A unified variational inference framework," *IEEE J. Sel. Areas Commun.*, vol. 43, no. 4, pp. 1339–1353, Apr. 2025.

[4] Y. Chen, D. He, H. Wang, W. Yuan, and T. Q. S. Quek, "Joint Channel and Clipping Amplitude Estimation and Signal Detection for Clipped OTFS," *IEEE Trans. Wireless Commun.*, 2025.

[5] D. Bergamasco, F. Clazzer, A. Munari and P. Casari, "A Low-PAPR Pilot Design and Optimization for OTFS Modulation," in *Proc. IEEE Int. Conf. Commun.*, Montreal, QC, Canada, 2025, pp. 976–982.

[6] X. Yang, B. Zhang, M. Zhou and M. Gao, "Integrated Sensing and Communications Waveform Design for OTFS and FTN Fusion," *IEEE Signal Process. Lett.*, vol. 31, pp. 2870–2874, 2024.

[7] Z. Hong, S. Sugiura, C. Xu and L. Hanzo, "Precoded Faster-Than-Nyquist Signaling Using Optimal Power Allocation for OTFS," *IEEE Wireless Commun. Lett.*, vol. 14, no. 1, pp. 173–177, Jan. 2025.

[8] P. Raviteja, K. T. Phan and Y. Hong, "Embedded Pilot-Aided Channel Estimation for OTFS in Delay–Doppler Channels," *IEEE Trans. Veh. Technol.*, vol. 68, no. 5, pp. 4906–4917, May 2019.

[9] L. Zhao, W. -J. Gao and W. Guo, "Sparse Bayesian Learning of Delay-Doppler Channel for OTFS System," *IEEE Commun. Lett.*, vol. 24, no. 12, pp. 2766–2769, Dec. 2020.

[10] Y. C. Pati, R. Rezaiifar, and P. S. Krishnaprasad, "Orthogonal matching pursuit: Recursive function approximation with applications to wavelet decomposition," in *Proc. 27th Asilomar Conf. Signals, Syst. Comput.*, 1993, pp. 40–44.

[11] X. Gong and J. Zheng, "Two-stage on-grid radar parameter estimation in OTFS based dual-function radar-communications," in *Proc. IEEE 24th Int. Workshop Signal Process. Adv. Wireless Commun. (SPAWC)*, Shanghai, China, Sep. 2023, pp. 36–40.

[12] O. Zacharia and M. Vani Devi, "Fractional delay and Doppler estimation for OTFS based ISAC systems," in *Proc. IEEE Wireless Commun. Netw. Conf. (WCNC)*, Glasgow, U.K., Mar. 2023, pp. 1–6.

[13] M. Ahmad, M. Sajid Sarwar and S. Y. Shin, "Deep-Learning-Assisted Channel Estimation for Adaptive Parameter Selection in mMIMO-SEFDM," *IEEE Internet Things J.*, vol. 12, no. 13, pp. 24174–24184, Jul., 2025.

[14] M. L. Ammari and P. Fortier, "Analysis of MIMO receiver using generalized least squares method in colored environments," *J. Comput. Netw. Commun.*, vol. 2014, pp. 1–6, Aug. 2014.

[15] R. Niazadeh, M. Babaie-Zadeh and C. Jutten, "On the Achievability of Cramér-Rao Bound in Noisy Compressed Sensing," *IEEE Trans. Signal Process.*, vol. 60, no. 1, pp. 518–526, Jan. 2012.